Computational Fluid Dynamic Simulation of Inhaled Radon Dilution by Auxiliary Ventilation in a Stone-Coal Mine Laneway and Dosage Assessment of Miners

Authors:

Bin Zhou, Ping Chang, Guang Xu

Abstract:

Inhaled radon status in the laneways of some Chinese stone-coal mines is a cause of concern. In this study, computational fluid dynamics simulations were employed to investigate three flowrates of the dilution gas (2.5, 5, and 7.5 m3/s) and radon distributions at realistic breathing levels (1.6, 1.75, and 1.9 m). The results showed that there are obvious jet-flow, backflow, and vortex zones near the heading face, and a circulation flow at the rear of the laneway. A high radon concentration area was found to be caused by the mining machinery. As the ventilation rate increased, the radon concentrations dropped significantly. An airflow of 7.5 m3/s showed the best dilution performance: The maximum radon concentration decreased to 541.62 Bq/m3, which is within the safe range recommended by the International Commission on Radiological Protection. Annual effective doses for the three air flowrates were 8.61, 5.50, and 4.12 mSv.

Record Type: Published Article

Citation (overall record, always the latest version):	LAPSE:2019.1099
Citation (this specific file, latest version):	LAPSE:2019.1099-1
Citation (this specific file, this version):	LAPSE:2019.1099-1v1

Computational Fluid Dynamic Simulation of Inhaled Radon Dilution by Auxiliary Ventilation in a Stone-Coal Mine Laneway and Dosage Assessment of Miners

Bin Zhou [1,2], Ping Chang [2,]* and Guang Xu [2]

[1] College of Safety and Emergency Management Engineering, Taiyuan University of Technology, Taiyuan 030024, China

[2] Department of Mining Engineering and Metallurgical Engineering, WA School of Mines: Minerals, Energy and Chemical Engineering, Curtin University, Kalgoorlie, WA 6430, Australia

* Correspondence: ping.chang@postgrad.curtin.edu.au; Tel.: +61-(0)452282422

Abstract: Inhaled radon status in the laneways of some Chinese stone-coal mines is a cause of concern. In this study, computational fluid dynamics simulations were employed to investigate three flowrates of the dilution gas (2.5, 5, and 7.5 m^3/s) and radon distributions at realistic breathing levels (1.6, 1.75, and 1.9 m). The results showed that there are obvious jet-flow, backflow, and vortex zones near the heading face, and a circulation flow at the rear of the laneway. A high radon concentration area was found to be caused by the mining machinery. As the ventilation rate increased, the radon concentrations dropped significantly. An airflow of 7.5 m^3/s showed the best dilution performance: The maximum radon concentration decreased to 541.62 Bq/m^3, which is within the safe range recommended by the International Commission on Radiological Protection. Annual effective doses for the three air flowrates were 8.61, 5.50, and 4.12 mSv.

Keywords: coal mining; radon concentration; ventilation; computational fluid dynamics; occupational exposure assessment

1. Introduction

^{222}Rn has recently drawn much attention, due to its radioactivity in underground workplaces which can cause over-exposure in miners [1,2]. ^{222}Rn (radon; Rn) is widely found in underground rocks as a product of uranium decay and can diffuse from rock pores to the working space during mining operations. Gaseous radon can become trapped in the lungs once inhaled, where it decays further and releases ionizing alpha particles. These high-energy particles can seriously damage the lung tissue and increase the probability of cell mutation leading to cancer [3].

To date, most radon research has focused on uranium mines, which have relatively high radon concentrations in the working environment. In the Colorado Plateau of the United States, radon concentrations in uranium mines can reach as high as 2.18×10^6 Bq/m^3 [4]. In the cut-and-fill stopes of a uranium mine in Canada, the radon concentrations varied in the range of 481–2960 Bq/m^3 [5]. All of these sites exceeded the action level (500–1500 Bq/m^3) for the workplace environment, as recommended by the International Commission on Radiological Protection (ICRP) [6]. Al-Zoughool et al. [7] assessed several studies on the radon exposure of uranium miners in six countries (U.S.A., Australia, Canada, France, Germany, and Czech Republic): the exposure of radon inhalation ranged from 7.6–595.7 working level months (WLM), which was much higher than the threshold limit of 4 WLM prescribed by the ICRP [8].

There have been few studies on radon occupational hazards for coal miners. This is mainly because the content of radionuclides in coal is low and good ventilation can usually maintain radon concentrations below the action level [9,10]. In some coal mines in China, however, the uranium content of the coal seams is relatively high and the mines are ventilation-poor, which leads to the potential risk of radon accumulation and radiological impacts on miners. Liu et al. [11] measured radon concentrations in 48 coal mines in twelve major coal-producing provinces in China. The results showed that there were greater radon concentrations in stone-coal mines without auxiliary ventilation. The concentrations ranged from 136–4183 Bq/m^3, with an average value of 1244 Bq/m^3. The typical value of radon concentrations of stone-coal mines in China was, therefore, suggested to be 1500 Bq/m^3, which is three times the lower limit of the action level (500 Bq/m^3). Stone coal is a type of anthracite with low carbon content, high ash content, low heat value, and which contains large amounts of pyrite, quartz, and phosphorus nodules [12]. The high uranium content of the mineral nodules and lack of effective ventilation are the major reasons that radon exceeds the limit in laneways of stone-coal mines. Occupational exposure of miners also requires attention, due to their long working hours (2400 h per year) [11].

Computational fluid dynamics (CFD), as a visual low-cost tool, has been widely used to solve health-related issues in the mining industry. Ren and Wang et al. [13,14] established a dust-removal model in a mine roadway and explored the impact of ventilation on dust contamination. The results illustrated that the area of high dust concentration shrank obviously, dropping by 72% when the airflow rate was increased from 7 m^3/s to 13 m^3/s. Kurnia et al. [15] designed three ventilation scenarios to investigate the relationship between airflow behavior and methane dispersion in a mine tunnel. The best methane mitigation was achieved at the maximum airflow rate. An actual ventilation shaft in a Chinese uranium mine was modeled by Xie et al. to predict radon radiation effects on surrounding residents [16]. As the wind speed increased from 0.5 m/s to 2 m/s, radon contamination within a range of 150 m from the shaft decreased from 600 Bq/m^3 to the limit of 100 Bq/m^3. At present, auxiliary ventilation is still the main way to effectively control toxic and harmful pollutants in an underground workplace. There are three main auxiliary ventilation systems used in coal mine laneways: Forcing ventilation systems, exhaust ventilation systems, and mixed ventilation systems (a forcing ventilation system together with an exhaust ventilation system); the forcing ventilation system being the most commonly used [17–19]. It is, therefore, important to understand airflow behavior in the laneway to select proper ventilation parameters to maintain radon concentrations at a reasonable level.

In this study, the airflow behavior in a typical laneway was simulated and analyzed by the OpenFOAM (Open Source Field Operation and Manipulation) CFD software at three ventilation rates (2.5 m^3/s, 5 m^3/s, and 7.5 m^3/s). Based on the obtained flow field, the scalarTransport equation was used to investigate the radon distribution at three respirable heights (1.6 m, 1.75 m, and 1.9 m). The optimal ventilation rate was, then, suggested for radon mitigation in the working area, according to the maximum radon results obtained from the various models. In addition, taking into account the working time over one year, the maximum annual effective dose received by miners was assessed. The study results are helpful for obtaining a better understanding of the complex airflow characteristics and radon dispersion under auxiliary ventilation and provides reliable guidance and education for the design of effective radon dilution systems.

2. Mathematical Formulation

2.1. Numerical Model

As the radon concentration data in this paper were derived from the statistical results of a survey of 48 coal mines in China [11], there are no specific laneway parameters to establish models for CFD research. For the purpose of this study, a typical laneway geometry and three ventilation parameters (2.5 m^3/s, 5 m^3/s, and 7.5 m^3/s), as used in the prior research by Shi et al. [20], were adopted to establish a numerical model for radon dilution performance research. Figure 1 illustrates the geometry of the

underground laneway model, which includes a ventilation duct, a heading face, and mining machinery. The length of the laneway is 50 m and the shape of the laneway section is a semicircular arch, where the upper semicircular radius is 2.75 m and the width and height of the lower rectangle are 5.5 m and 1.05 m, respectively. The body shape of the machinery is roughly $10 \times 3.6 \times 1.8$ m. The ventilation duct, with a length of 43 m and a diameter of 0.8 m, is suspended on the side of the laneway; its distance from the ground is 2.5 m and the distance from the wall is 0.2 m. The distance between the outlet of the duct and the mining face is 7 m.
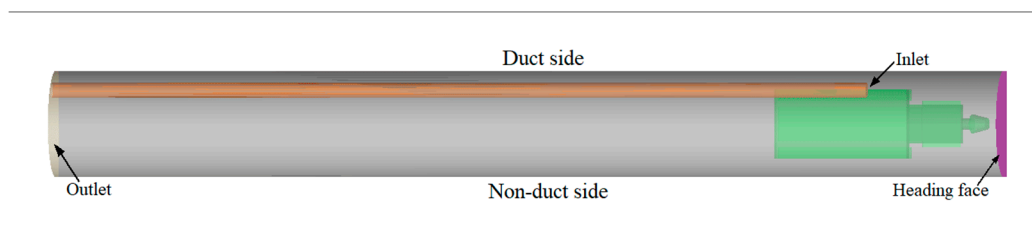
Figure 1. The geometry of underground laneway [20].

Following the construction of the model geometry, the computational domain was meshed. A structured mesh generally has a higher quality, which is suitable for simple and regular geometric models, while an unstructured mesh has relatively lower quality and is applied to complex geometric models. According to the geometric structure of the laneway model, hybrid meshes were selected and established by ICEM (Integrated Computer Engineering and Manufacturing code for computational fluid dynamics). The thickness of the outermost boundary layer was 0.005 m, the number of layers was 6, and the scale factor between adjacent layers was 1.2. A structural mesh was adopted in the domain behind the mining machinery with a quality exceeding 0.5, while an unstructured mesh was used in the rest of the domain with quality greater than 0.3; both mesh qualities met the requirements of the OpenFOAM software for simulation.

2.2. Boundary Conditions

The standard wall function was applied on the walls of the laneway and the mining machinery. A velocity-type inlet was adopted in the duct outlet to simulate the fresh air inlet of the laneway, and the ventilation airflow rates were 2.5 m^3/s, 5 m^3/s, and 7.5 m^3/s. A pressure outlet was adopted in the outlet of the laneway, where the outlet pressure was treated as a standard atmospheric pressure (101 kpa). The radon source was set to 1500 Bq/m^3·s and the diffusion coefficient of radon was set to 1.1×10^{-5} m^2/s. The air density, dynamic viscosity, and kinematic viscosity were set as 1.213 kg/m^3, 1.811×10^{-5} Pa/s, and 1.503×10^{-5} m^2/s, respectively. A turbulence intensity of 5% was applied in all ventilation scenarios.

2.3. Governing Equations

In the underground coal mine, a large amount of fresh air is forced into the laneway space by the ventilation duct, which increases the Reynolds number of the airflow in the laneway. The standard k-ε turbulence model, a common turbulence model, was used in this OpenFOAM simulation. The k-ε model has been used by many scholars [13,18,21] for ventilation research in coal-mining related fields. It has been shown that the simulation results of the k-ε model are highly consistent with the field measured data. The air in the laneway was considered as an incompressible ideal gas and the effects of heat exchange and humidity on the airflow field were ignored. It is clear that the radon migration under the auxiliary ventilation in the laneway is very dynamic and will be affected by several ventilation parameters related to time and the facilities and, so, the steady-state assumption is not strictly valid. However, the computing costs, including grid quality, computer configuration, and computation time, especially in large 3D models, make time-dependent computational simulations difficult to

implement. Moreover, the radiation hazard suffered by miners in the underground laneway is a long-term accumulation process. The annual radiation dose received by miners is estimated on the basis of a relatively stable radon concentration, so it is not of much concern to consider the fluctuations in radon concentration over a short period of time. Many previous studies [22–24] have also used measured data to justify the steady-state assumption model, and the comparison results showed that the model results and the measured results were highly consistent. Based on this, simpleFoam, a stable solver using the SIMPLE (semi-implicit method for pressure-linked equations) algorithm, was adopted to reach a steady-state airflow field ahead of the mining operation [25]. In the radon dispersion section, radon was assumed to have a negligible effect on the airflow fields, because its mass is very small compared with that of air (1 Bq/m^3 = 1.75 × 10^{-19} kg/m^3), the radon concentration of the ventilated air is also not considered. The radon concentration field could, therefore, be obtained using scalarTransportFoam, which is a solver for passive scalar transport in a given velocity field [26]. Transport equations for mass, momentum, and concentration of species were described, following [27].

The airflow is governed by the continuity and Navier–Stokes equations:

$$\frac{\partial \rho}{\partial t} + \nabla \cdot (\rho U) = 0, \tag{1}$$

$$\rho \left(\frac{\partial U}{\partial t} + U \cdot \nabla U \right) = -\nabla P + \mu_e \nabla^2 U, \tag{2}$$

where ρ is the air density, kg/m^3; U is the air velocity, m/s; P represents the pressure, N/m^2; and μ_e represents the effective viscosity, N/m^2·s, which is the sum of the dynamic and turbulent viscosities.

The radon motion was governed by the scalarTransport equation:

$$\frac{\partial C}{\partial t} + \nabla \cdot (UC) - \nabla \cdot (D * \nabla C) - \lambda C + S = 0, \tag{3}$$

where C is the radon concentration in the laneway, Bq/m^3; D is the Rn diffusion coefficient, m^2/s; S is the radon source item, Bq/m^3; and λ is radon decay coefficient, 2.1 × 10^{-6} s^{-1}.

2.4. Assessment of Occupational Exposure to Inhaled Radon

To evaluate the inhaled radon exposure of miners, three respirable heights were assessed, according to the range of miner heights. Combining the maximum radon concentration in the working area and average working time in one year, the maximum annual effective dose of radon inhalation was assessed using the following equation [28]:

$$E_{eff} = C_{R_n max} \times D_f \times T \times F, \tag{4}$$

where E_{eff} represents the maximum annual effective dose, mSv; $C_{R_n max}$ represents the maximum radon concentration in the activity area of workers, Bq/m^3; D_f is the dose conversion factor, 9.0 × 10^{-6} mSv/h per Bq/m^3; T is the annual number of working hours, h; and F is the equilibrium factor, which was set to 0.35 for a coal mine [29].

3. Mesh Independence Study

A mesh independence study considers the effect of the number of model cells on the numerical solution, which is essential in CFD modeling. Mesh refinement can reduce the probability of solution divergence and ensure that the numerical results approach the exact solution of the governing equations [30]; however, unnecessarily increasing the number of model cells reduces solution efficiency, thereby wasting computational resources [31]. To minimize the impact of the mesh on the calculation accuracy and to select a suitable number of cells to ensure adequate convergence speed, a medium mesh, with about 2 million cells, and a fine mesh, with about 4 million cells, were built. An airflow field

with a ventilation rate of 5 m^3/s was adopted and the velocity features of three monitoring lines were taken into account to assess the mesh independence: The monitoring lines 1, 2, and 3 were located on the horizontal central lines of the laneway, and the distances from the outlet were 10 m, 30 m, and 48 m, respectively, as shown in Figure 2. The results of the mesh independence study are plotted in Figure 3.
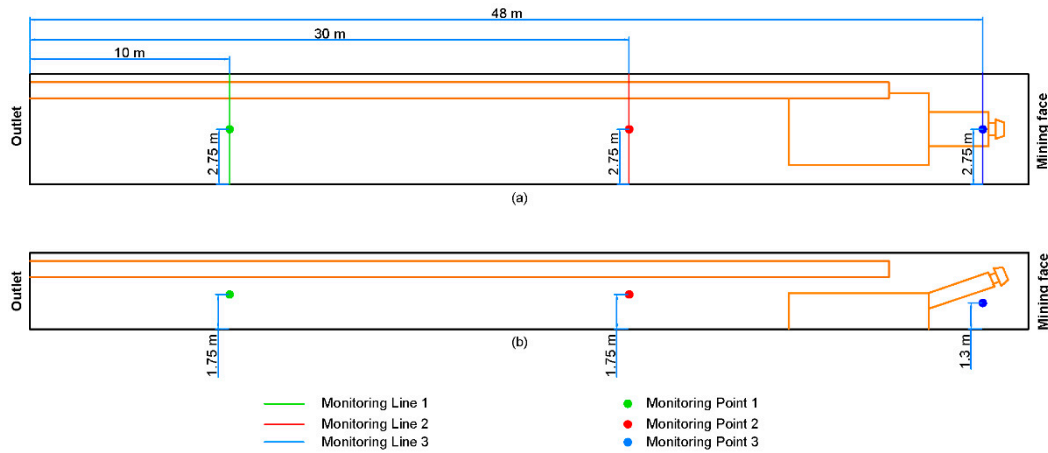
Figure 2. Position of monitoring lines and points.
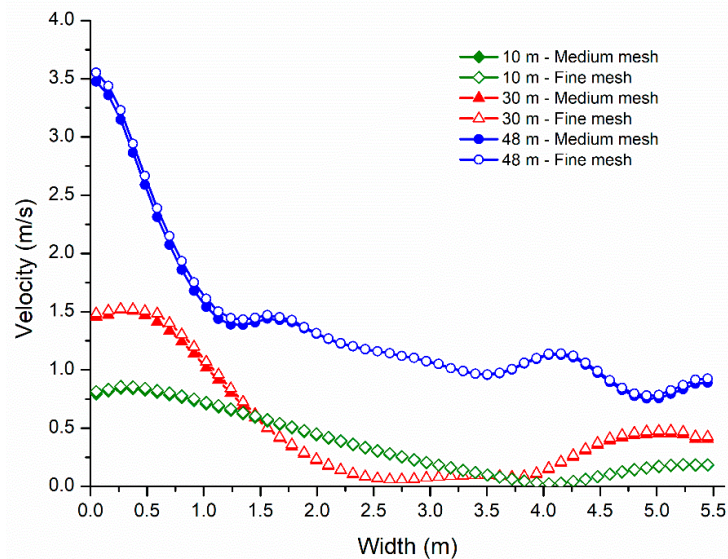
Figure 3. Airflow velocities at monitoring lines.

The velocity profiles at each position approximately coincided for the two meshes. This indicated that the medium mesh had little effect on the accuracy of the domain calculation and met the requirement for mesh independence. Therefore, the medium mesh with 2 million cells, as shown in Figure 4, was used for subsequent airflow field research and radon dispersion analysis.
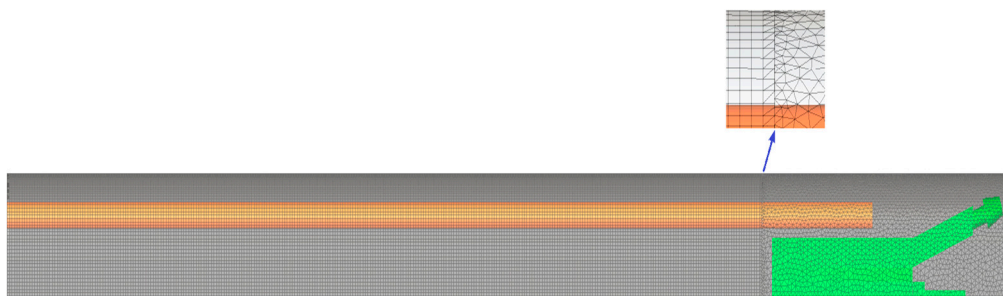
Figure 4. Laneway model using medium mesh.

4. Judging Criteria for Concentration Field Convergence

The criteria for the convergence of the radon concentration field were as follows: (1) To guarantee the solution was converged, the residual value of the concentration governing equation needed to reach 1×10^{-8}. (2) Three monitoring points were set to observe the concentration change and the concentration field was considered to reach a steady state when the concentrations at the three points no longer changed with the iteration. The first monitoring point (10, 2.75, 1.75) was located near the laneway outlet; the second monitoring point (30, 2.75, 1.75) was located behind the mining machinery; and the third monitoring point (48, 2.75, 1.3) was located on the side of the machinery. The radon concentration change at the three points is plotted in Figure 5. As can be seen from Figure 5, the radon concentrations at the three points remained the same after 1000 iterations and, thus, the radon concentration field after this time was considered to reach a steady state.
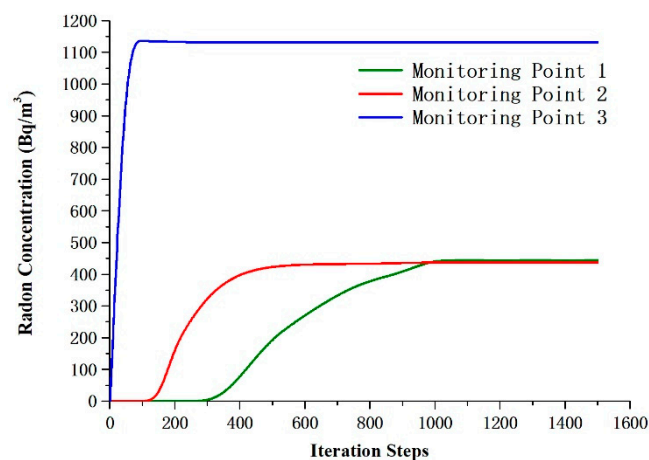

**Figure 5.** Radon concentration change at the monitoring points.

5. Results and Discussion

5.1. Airflow Characteristics and Distributions at Breathing Levels

An auxiliary ventilation system in an underground mine is usually employed to blow high-speed air into the workplace through a ventilation duct. The fresh air not only supplies miners with oxygen, but also removes toxic and harmful gases that are released during the mining process. The airflow characteristics must, therefore, be well understood before investigating the radon distribution. Figure 6 shows a streamline diagram of the airflow field in the laneway (ventilation rate: 2.5 m³/s).

Previous research [32,33] has demonstrated that auxiliary ventilation in a laneway is a turbulent jet flow in a finite space: Three zones (the jet-flow, backflow, and vortex zones) form in the laneway. A similar trend was observed in this study. Figure 6 shows that the high-speed air blown into the laneway from the ventilation duct forms a distinct jet-flow zone on the duct side. The velocity of the jet flow decreases gradually as it progresses toward the mining face. When the airflow reaches

the heading face, the flow direction changes and the air disperses on the heading face, due to the heading face block. When it reaches the heading face edge, the airflow then changes direction again and flows back toward the laneway outlet. On the downstream side, the backflow is separated due to the presence of mining machinery. Most of the backflow moves toward the laneway outlet through the narrow space on the sides of the mining machinery. A small part of the backflow is blocked by the equipment and forms a vortex zone in the excavation space. A distinct circulation flow is generated, due to the combined effects of the separated airflows at the rear of the laneway. The low velocity and its recirculating nature may greatly weaken the radon removal capacity of the airflow, contributing to potential radon accumulation in this area. The above phenomena are in agreement with the results of numerical studies by Wang et al. and Qin et al. [34,35].
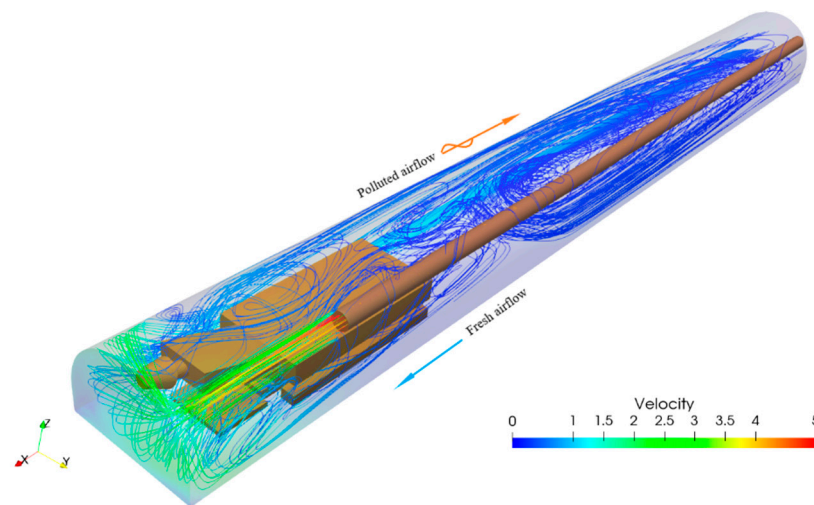
Figure 6. Streamline diagram of the airflow field in the laneway.

Referring to previous studies [34,36], 2.5 m^3/s, 5 m^3/s, and 7.5 m^3/s were selected as the airflow rates from the ventilation duct in the simulation. Different respirable heights were investigated to understand airflow distributions at these breathing levels. The airflow profiles on the horizontal cross-sections are shown in Figure 7. Cases 1, 2, and 3 represent the steady-state airflow fields of the laneway when the ventilation rates of the duct were 2.5 m^3/s, 5 m^3/s, and 7.5 m^3/s, respectively.
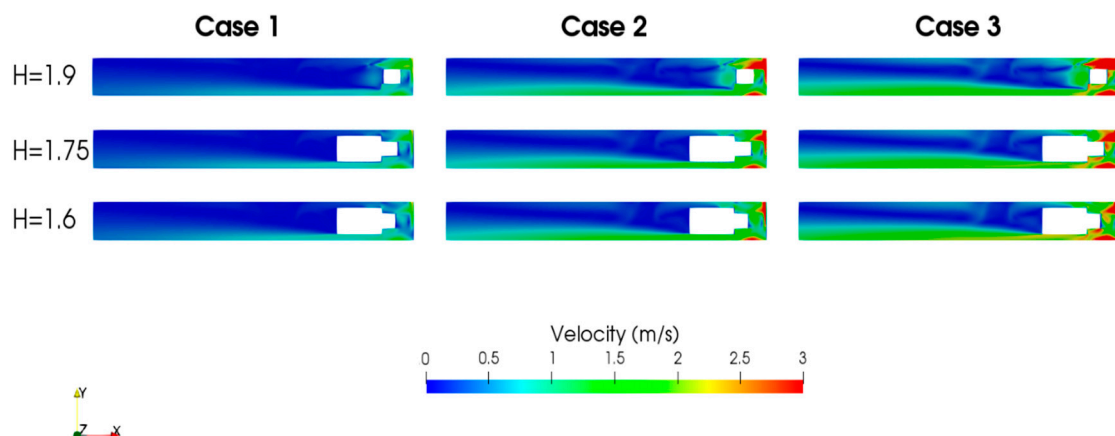
Figure 7. Effect of the ventilation rates on the horizontal cross-sectional distribution of airflow fields at different respirable heights.
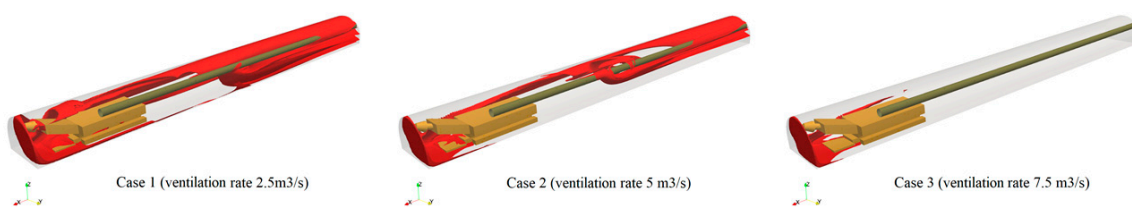
For each case, the airflow dispersion patterns were similar at different breathing heights; the areas with the most intense airflow were mainly located in the space between the machinery and the mining

face on the return side. This is because the airflow forced into the laneway will first accumulate in the mining space in front of the machinery, resulting in a sharp increase in airflow velocity. Then, obstructed by the wall on the duct side and the mining face, the airflow moved to the space on the non-duct side, and eventually flowed towards the laneway outlet along the wall. However, some slight changes in the jet-flow zone are worth noting. As can be seen from Figure 7, with an increase of respirable height, the high-velocity area of the jet flow expanded continuously. The main reason for this is that the location of the ventilation duct is near the roof, so the loss of airflow velocity near the duct is small. In the rear of the laneway, a distinct recirculation area was formed due to the presence of the machinery and the lower velocity of the airflow. With an increase of the ventilation rate, the airflow distribution changed markedly. A large amount of airflow in the restricted mining space bypassed the machinery and flowed rapidly to the rear of the laneway. As a result, the airflow rates on both sides of the laneway were obviously accelerated, the areas influenced by the airflow became longer and wider, and the recirculation area between both sides was less compressed.

5.2. Distribution of Radon Concentration Field

Figure 8 gives radon concentrations when the ventilation rates were 2.5 m^3/s, 5 m^3/s, and 7.5 m^3/s. The red contour represents the value of radon concentration equal to or exceeding 500 Bq/m^3, which is the lower limit of the action level (500–1500 Bq/m^3) required by the ICRP. It can be seen that the radon high-concentration areas were mainly located on the non-duct side and the rear of the laneway, and the whole high-concentration area of radon accounted for about 50% of the laneway space. This is because the radon gas released from the mining face was diluted by the fresh air, then radon gas was carried by the airflow to flow downstream. The radon concentration will increase dramatically due to the sharp reduction of space when flowing through the mining machinery. In addition, as distance increased, the airflow weakened at the rear of the laneway, which exacerbated the formation of circulation zones and caused radon gas to build up in those zones.


Case 1 (ventilation rate 2.5m3/s)   Case 2 (ventilation rate 5 m3/s)   Case 3 (ventilation rate 7.5 m3/s)

Figure 8. Radon distribution with concentrations ≥ 500 Bq/m^3.

With the increase of the ventilation flow rate, the high-concentration areas of radon in the laneway had a significant trend of decrease. When the ventilation rate increased to 7.5 m^3/s, the high-concentration areas only accumulated near the mining face, and the radon concentration at the rear of the laneway was diluted to below 500 Bq/m^3. The simulation results demonstrated that radon dispersion was highly affected by the airflow pattern.

To better understand the radon distribution in the laneway under the auxiliary ventilation, the radon concentration at different cross-sectional planes were further analyzed.

Figure 9 shows the radon concentration distributions of different respirable heights in horizontal cross-section planes. In Case 1, the radon concentration was relatively high near the heading face, due to the existence of circulation. When the ventilation flow rates were increased to 5 m^3/s and 7.5 m^3/s in Cases 2 and 3, respectively, the radon dilution effect of the airflow was enhanced and radon was quickly removed by the faster airflow, so the circulation area progressively shrank and the radon concentration gradually dropped. When the airflow moved to the non-duct side of the laneway, there was an obvious high radon concentration area between the mining machinery and the non-duct side, mainly because the mining equipment caused a sharp contraction of the airflow space. With the airflow rate increased, the movement of the airflow in the narrow space was strengthened and more radon was carried downstream, which would create a better working environment for the operators.

When the airstream emerged from the tail of the machinery, the flow velocity dropped significantly and eventually formed a circulating flow at the rear of the laneway. As discussed above, radon could not be efficiently removed from the laneway because of the circulation flow and, instead, accumulated in this area. As the airflow increased, radon was carried downstream more efficiently, rather than being captured by the flow circulation; this resulted in a significant reduction in radon concentration at the rear of the laneway.
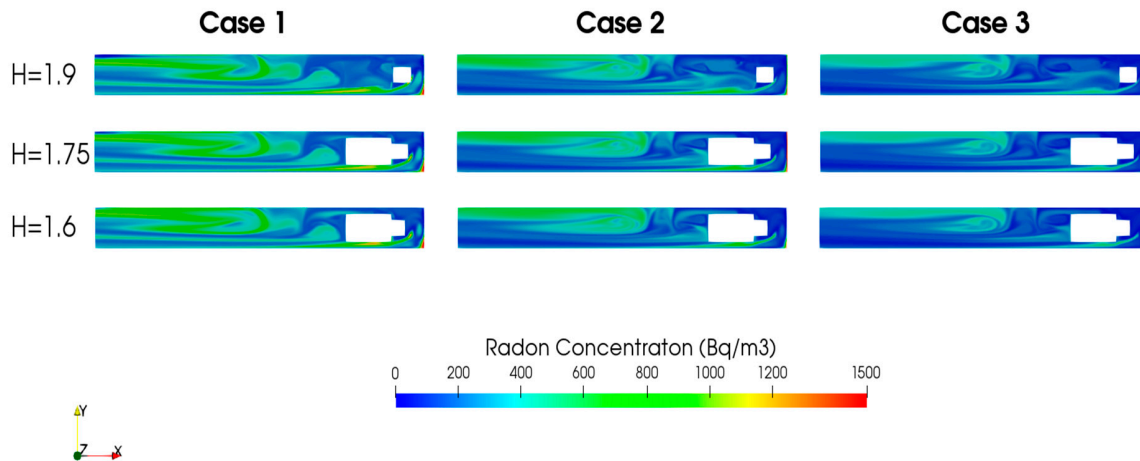
Figure 9. Horizontal cross-sections of radon concentration distribution at different ventilation rates and respirable heights.

Figure 10 shows the distribution of radon concentration in vertical cross-sections at different locations from the heading face. Radon gas released from the heading face was firstly transported along the non-duct side and then diffused into the entire space behind the mining machinery. Closer inspection revealed that the high radon concentration area throughout the laneway was mainly located near the machinery, because of the limited space.

Take the vertical cross-section plane of radon concentration 7 m from the mining face as an example. When the ventilation rate was 2.5 m^3/s, most of the radon gas was blown to the non-duct side of the laneway, resulting in a radon accumulation in this area. The radon concentration in the respirable height range (1.6–1.9 m) was around 400–1200 Bq/m^3, and a small amount of radon gas was distributed in the upper space of the machinery. With an increase of air quantity, more radon gas was discharged from the laneway outlet and the high-concentration area of radon decreased continuously; thus, radon pollution was effectively controlled. Although the radon concentration in the breathing area was still relatively high, the range of radon concentration in this area was decreased to about 300–700 Bq/m^3 when the airflow rate was 5 m^3/s. The ventilation scenario with the flowrate of 7.5 m^3/s obtained the best radon removal performance in this study. It can be seen that the radon concentration distribution in the cross-section plane was relatively uniform, which indicates that radon gas was removed from the laneway space in a timely manner by the high-speed airflow. The radon concentration on the entire section plane had almost dropped below the threshold action level of 500 Bq/m^3.
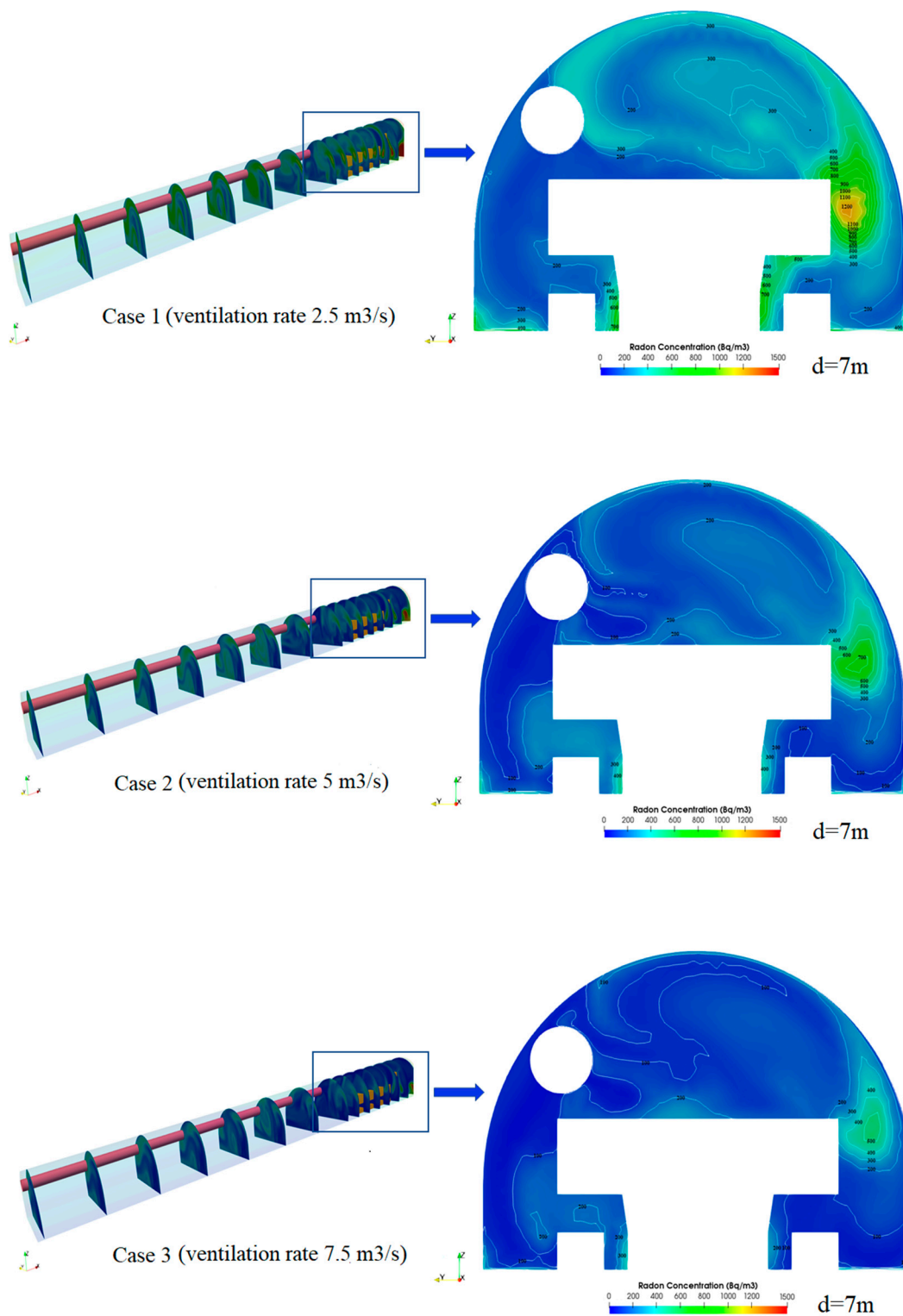
Figure 10. Vertical cross-sections of radon concentration distribution at different locations from the heading face.

5.3. Assessment of Occupational Exposure to Radon Inhalation

There are many different types of work in the underground laneway, such as mining machinery driver, equipment maintainer, electrician, hauler, support worker, and safety supervisor. Most activity occurs on the non-duct side, due to the existence of the duct on the other side. Compared with other types of work, the mining machinery driver is the closest to the heading face and is located in the

narrow space near the machinery on the non-duct side for remotely driving and ensuring that the mining direction meets the operation requirements. The narrow working space benefits the radon accumulation, but it also increases the airflow rate for radon migration. Therefore, the working area of the driver becomes a key area for radon pollution monitoring; the radon dilution performance under different ventilation rates and annual effective dose assessment for the machinery driver is, hence, worthy of investigation.

In this study, the driver's working area—the space between the mining machinery and the non-duct side—was regarded as the working area of the laneway. As the overall width of the laneway was 5.5 m and the width of the mining machine was 3.6 m, the width of the driver's working area was about 1 m ((5.5 − 3.6)/2 = 0.95 m) which was only just enough for a machinery driver to work properly. Therefore, the driver's breathing height was defined as the center of the working area with width (y = 1/2 = 0.5 m) and height H = 1.6, 1.75, or 1.9 m above the ground. The inhaled radon concentrations along the non-duct side of laneway at different ventilation rates are shown in Figure 11.
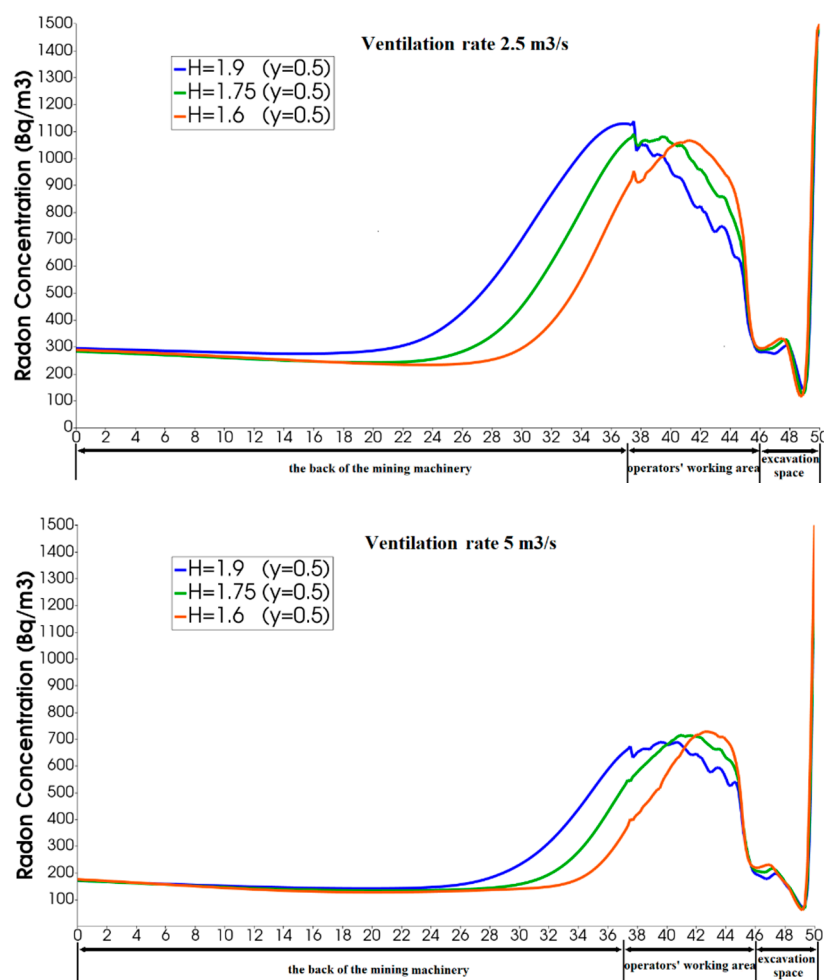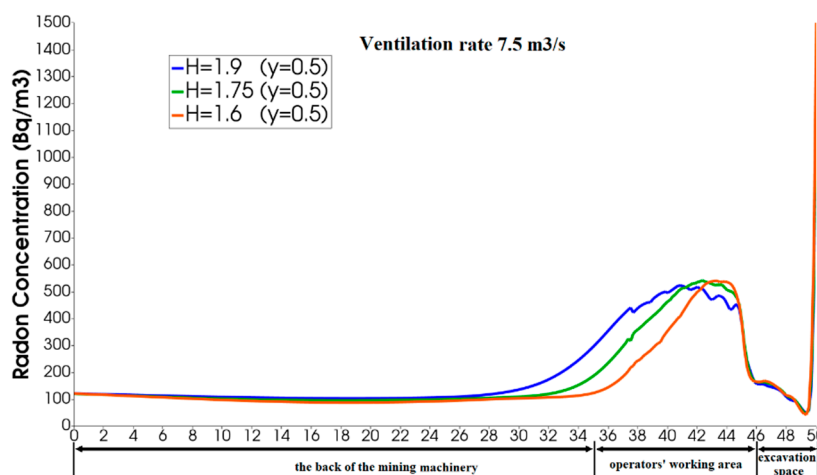

Figure 11. *Cont.*

Figure 11. Inhaled radon concentrations along the non-duct side of laneway at different ventilation rates.

As the distance increased from the heading face, the radon concentration first dropped sharply in the excavation space, then rose rapidly in the working area, and finally decreased to a relatively low concentration at the back of the mining machinery. In all cases, the area with the highest radon concentration was mainly concentrated in the work area. There was a negligible effect of breathing height on the maximum radon value, but there was a significant influence of airflow field. In Case 1, the highest radon concentration was 1138.25 Bq/m^3. As the ventilation rate increased to 5 m^3/s, in Case 2, the radon concentration in the workplace was lower, but not adequately mitigated: The maximum radon was still as high as 727.79 Bq/m^3. Case 3, with a ventilation rate of 7.5 m^3/s, offered the best radon management result: The peak radon concentration was 541.62 Bq/m^3, which was almost at the lower limit of the action level (500–1500 Bq/m^3) for a workplace environment, as required by the ICRP.

According to Equation (4), the maximum effective dose for miners is not only related to maximum concentration in the working place, but also affected by the working hours. The results are shown in Table 1. The maximum annual effective doses for the three cases were 8.61 mSv, 5.50 mSv, and 4.12 mSv, respectively, all of which were below the statutory limit of 20 mSv for workers in the working place, as prescribed by the ICRP [37].

Table 1. Annual effective radon dose to miners.

	Ventilation Rate of the Duct (m^3/s)	Maximum Radon Concentration in the Workplace (Bq/m^3)	Annual Working Time (h)	Annual Effective Dose (mSv)
Case 1	2.5	1138.25	2400	8.61
Case 2	5	727.79	2400	5.50
Case 3	7.5	541.62	2400	4.12

5.4. CFD Modeling Limitations

Model validation is a very important part of related CFD studies, guaranteeing the accuracy of simulation results and the reliability of prediction results. However, as previously mentioned, this study was based on the statistical data of radon concentrations in the underground laneways of 48 coal mines in China, collected by Liu et al. [11], and so there were no specific laneway parameters to conduct a numerical model and no field-measured results for model validation. For the purpose of this research, a typical model simplified from an underground laneway in the Tangshan Donghua Coal Mine, China [20] and relative ventilation parameters were adopted to study the airflow distribution and radon migration under auxiliary ventilation. These simulation results could provide education for better understanding airflow characteristics in the laneway and inform guidelines for prevention and control of radioactive disasters in stone-coal mines.

6. Conclusions

In this study, a typical laneway model with forcing ventilation was established to evaluate the effectiveness of three different ventilation systems on radon concentration. The airflow pattern and radon concentration distributions were presented for each ventilation system. Results showed that the airflow fields of the laneway were distributed unevenly. There was an apparent jet-flow area on the duct side, a backflow area on the non-duct side, and circulation areas in the excavation space and at the rear of the laneway. With an increase of ventilation rate, the jet-flow and backflow zones were strengthened and expanded, while the circulation zones were diminished. This phenomenon is consistent with the results of previous studies.

The airflow pattern in the laneway played a key role in the radon concentration distribution. When the radon gas was released into the excavation space from the mining face, it was continuously diluted by the large quantities of fresh airflow. Then, most of the radon gas was carried by the airflow and moved rapidly toward the outlet of the laneway along the non-duct side. As the distance increased, the airflow velocity dropped markedly, which resulted in a big circulation area at the rear of the machinery. Radon gas that flowed with the airflow was also trapped by the circulation, eventually forming a high radon concentration area.

With an increase of ventilation quantity, the radon concentration in the laneway decreased significantly. In case 3, with a ventilation rate of 7.5 m^3/s, the best radon control performance was observed: The radon concentrations at respirable heights were reduced below the limit of the action level for the working place. The annual effective doses received by miners in all three cases were less than the limit of 20 mSv prescribed by the ICRP.

This study highlights the importance of auxiliary ventilation in effectively controlling the radon concentration in an underground laneway, which is crucial for the prevention of underground radioactive hazards. As model validation was not conducted in this study, it is recommended to compare and verify simulation results with measured data in future research.

References

1. United Nations; Scientific Committee on the Effects of Atomic Radiation. *Report of the United Nations Scientific Committee on the Effects of Atomic Radiation: Fifty-sixth Session (10–18 July 2008)*; United Nations Publications: San Francisco, CA, USA, 2008.

2. Vogiannis, E.G.; Nikolopoulos, D. Radon sources and associated risk in terms of exposure and dose. *Front. Public Health* **2015**, *2*, 207. [CrossRef] [PubMed]

3. Ting, D.S.K. *WHO Handbook on Indoor Radon: A Public Health Perspective*; Taylor & Francis: Milton Park, UK, 2010.

4. Joseph, K.; Wagoner, M.S.; Victor, E.; Archer, M.D.; Benjamin, E.; Carroll, M.A.; Duncan, A.; Holaday, M.A.; Pope, A.; Lawrence, M.S. Cancer mortality patterns among US uranium miners and millers, 1950 through 1962. *J. Natl. Cancer Inst.* **1964**, *32*, 787–801.

5. Cheng, K.C.; Porritt, J.W.M. The measurement of radon emanation rates in a Canadian cut-and-fill uranium mine. *CIM (Can. Inst. Min. Metall.) Bull* **1981**, *74*, 110–118.

6. Valentin, J. The 2007 recommendations of the international commission on radiological protection. *Ann. ICRP* **2007**, *7*, 1–332.

7. Al-Zoughool, M.; Krewski, D. Health effects of radon: A review of the literature. *Int. J. Radiat. Biol.* **2009**, *85*, 57–69. [CrossRef] [PubMed]

8. Cousins, C.; Miller, D.; Bernardi, G.; Rehani, M.; Schofield, P.; Vañó, E.; Einstein, A.; Geiger, B.; Heintz, P.; Padovani, R.J.I.P. International commission on radiological protection. *J. ICRP Publ.* **2011**, *120*, 1–125.

9. Qureshi, A.A.; Kakar, D.M.; Akram, M.; Khattak, N.U.; Tufail, M.; Mehmood, K.; Jamil, K.; Khan, H.A. Radon concentrations in coal mines of Baluchistan, Pakistan. *J. Environ. Radioact.* **2000**, *48*, 203–209. [CrossRef]

10. Baldık, R.; Aytekin, H.; Çelebi, N.; Ataksor, B.; Taşdelen, M. Radon concentration measurements in the AMASRA coal mine, Turkey. *Radiat. Prot. Dosim.* **2005**, *118*, 122–125.

11. Liu, F.D.; Pan, Z.Q.; Liu, S.L.; Chen, L.; Ma, J.Z.; Yang, M.L.; Wang, N.P. The estimation of the number of underground coal miners and the annual dose to coal miners in China. *Health Phys.* **2007**, *93*, 127–132. [CrossRef]

12. Dai, S.; Zheng, X.; Wang, X.; Finkelman, R.B.; Jiang, Y.; Ren, D.; Yan, X.; Zhou, Y. Stone coal in China: A review. *Int. Geol. Rev.* **2018**, *60*, 736–753. [CrossRef]

13. Wang, Z.; Ren, T. Investigation of airflow and respirable dust flow behaviour above an underground bin. *Powder Technol.* **2013**, *250*, 103–114. [CrossRef]

14. Ren, T.; Wang, Z.; Cooper, G. CFD modelling of ventilation and dust flow behaviour above an underground bin and the design of an innovative dust mitigation system. *Tunn. Undergr. Space Technol.* **2014**, *41*, 241–254. [CrossRef]

15. Kurnia, J.C.; Sasmito, A.P.; Mujumdar, A.S. CFD simulation of methane dispersion and innovative methane management in underground mining faces. *Appl. Math. Model.* **2014**, *38*, 3467–3484. [CrossRef]

16. Xie, D.; Wang, H.; Kearfott, K.J.; Liu, Z.; Mo, Z. Radon dispersion modeling and dose assessment for uranium mine ventilation shaft exhausts under neutral atmospheric stability. *J. Environ. Radioact.* **2014**, *129*, 57–62. [CrossRef] [PubMed]

17. Kissell, F.; Wallhagen, R. Some new approaches to improve ventilation of the working face. In Proceedings of the NCA/BCR Coal Conference, Louisville, KY, USA, 19–21 October 1976.

18. Toraño, J.; Torno, S.; Menendez, M.; Gent, M.; Velasco, J. Models of methane behaviour in auxiliary ventilation of underground coal mining. *Int. J. Coal Geol.* **2009**, *80*, 35–43. [CrossRef]

19. Schultz, M.J.; Beiter, D.A.; Watkins, T.R.; Baran, J.N. *Face Ventilation Investigation: Clark Elkorn Coal Company*; Pittsburgh Safety and Health Technology Center Ventilation Division: London, UK, 1993.

20. Shi, G.; Liu, M.; Guo, Z.; Hu, F.; Wang, D. Unsteady simulation for optimal arrangement of dedusting airduct in coal mine heading face. *J. Loss Prev. Process. Ind.* **2017**, *46*, 45–53. [CrossRef]

21. Kurnia, J.C.; Sasmito, A.P.; Mujumdar, A.S. Simulation of a novel intermittent ventilation system for underground mines. *Tunn. Undergr. Space Technol.* **2014**, *42*, 206–215. [CrossRef]

22. Hargreaves, D.M.; Lowndes, I.S. The computational modeling of the ventilation flows within a rapid development drivage. *Tunn. Undergr. Sp. Tech.* **2007**, *22*, 150–160. [CrossRef]

23. Whittles, D.; Lowndes, I.S.; Kingman, S.W.; Yates, C.; Jobling, S. Influence of geotechnical factors on gas flow experienced in a UK longwall coal mine panel. *Int. J. Rock Mech. Min.* **2006**, *43*, 369–387. [CrossRef]

24. Wang, H.; Wang, C.; Wang, D. The influence of forced ventilation airflow on water spray for dust suppression on heading face in underground coal mine. *Powder Technol.* **2017**, *320*, 498–510. [CrossRef]

25. Patankar, S. *Numerical Heat Transfer and Fluid Flow*; CRC Press: Boca Raton, FL, USA, 1980.

26. Pawlowski, S.; Nayaka, N.; Meireles, M.; Portugal, C.A.M.; Velizarov, S.; Crespo, J.G. CFD modelling of flow patterns, tortuosity and residence time distribution in monolithic porous columns reconstructed from X-ray tomography data. *Chem. Eng. J.* **2018**, *340*, 757–766. [CrossRef]

27. Chauhan, N.; Chauhan, R.P.; Joshi, M.; Agarwal, T.K.; Sapra, B.K. Measurements and CFD modeling of indoor thoron distribution. *Atmos. Environ.* **2015**, *105*, 7–13. [CrossRef]

28. UNSCEAR; Electro Optical Industries; United Nations Scientific Committee on the Effects of Atomic Radiation. *Sources and Effects Of Ionizing Radiation*; UNSCEAR: New York, NY, USA, 2000.

29. Chen, L.; Senlin, L.; Fudong, L.; Chunhong, W.; Yihua, W.; Jizeng, M.; Ziqiang, P. A primary assessment of occupational exposure to underground coal miners in China. *Radiat. Prot.* **2008**, *28*, 129–137.

30. Xu, G.; Edmund, C.J.; Kray, D.L.; Saad, A.R.; Michael, E.K. Remote characterization of ventilation systems using tracer gas and CFD in an underground mine. *Saf. Sci.* **2015**, *74*, 140–149. [CrossRef]

31. Sarkar, J.; Shekhawat, L.K.; Loomba, V.; Rathore, A.S. CFD of mixing of multi-phase flow in a bioreactor using population balance model. *Biotechnol. Prog.* **2016**, *32*, 613–628. [CrossRef] [PubMed]

32. Wang, H.; Shi, S.; Liu, R. Numerical simulation study on ventilation flow field of wall-attached jet in heading face. *J. China Coal Soc.* **2004**, *4*, 011.

33. Jian-Liang, G.; Yan, X.K.-l.W. Numerical experiment of methane distribution in developing roadway. *China Saf. Sci. J. (CSSJ)* **2009**, *1*, 005.

34. Wang, Y.; Lou, G.; Geng, F.; Li, Y.B.; Li, Y.L. Numerical study on dust movement and dust distribution for hybrid ventilation system in a laneway of coal mine. *J. Loss Prev. Process Ind.* **2015**, *36*, 146–157. [CrossRef]

35. Qin, Y.; Jiang, Z.; Zhang, M. Comparison of simulation on dust migration regularity in fully mechanized workface. *Chin. J. Liaoning Tech. Univ.* **2014**, *33*, 289–293.

36. Lu, Y.; Akhtar, S.; Sasmito, A.; Kurnia, J.C. Numerical study of simultaneous methane and coal dust dispersion in a room and pillar mining face. In Proceedings of the 3rd International Symposium on Mine Safety Science and Engineering, Montreal, QC, Canada, 13–19 August 2016.

37. Lario, J.; Sánchez-Moral, S.; Cañaveras, J.C.; Cuezva, S.; Soler, V. Radon continuous monitoring in Altamira Cave (northern Spain) to assess user's annual effective dose. *J. Environ. Radioact.* **2005**, *80*, 161–174. [CrossRef]